Effect of doping concentration on the performance of terahertz quantum-cascade lasers

H. C. Liu,[a)] M. Wächter, D. Ban, Z. R. Wasilewski, M. Buchanan, and G. C. Aers
Institute for Microstructural Sciences, National Research Council, Ottawa K1A 0R6, Canada

J. C. Cao and S. L. Feng
State Key Laboratory of Functional Materials for Informatics, Shanghai Institute of Microsystem and Information Technology, Chinese Academy of Sciences, Shanghai 200050, China

B. S. Williams and Q. Hu
Department of Electrical Engineering and Computer Science and Research Laboratory of Electronics, Massachusetts Institute of Technology, Cambridge, Massachusetts 02139

(Received 8 February 2005; accepted 8 August 2005; published online 26 September 2005)

We characterized a set of terahertz quantum-cascade lasers with identical device parameters except for the doping concentration. The δ-doping density was varied from 3.2×10^{10} to 4.8×10^{10} cm^{-2}. We observed that the threshold current density increased monotonically with doping. Moreover, the measured results on devices with different cavity lengths provided evidence that the free carrier absorption caused waveguide loss also increased monotonically. Interestingly, however, the observed maximum lasing temperature displayed an optimum at a doping density of 3.6×10^{10} cm^{-2}. © *2005 American Institute of Physics*. [DOI: 10.1063/1.2067699]

Since Köhler *et al.* reported a quantum-cascade laser (QCL) operating in the terahertz (THz) frequency range at 4.4 THz,[1] significant progress has been made over the past three years.[2,3] For example, THz QCLs have been improved from lasing only at very low temperatures[1,2] to 164 K (Ref. 4) and from operating only in pulsed mode[1–3] to continuous wave.[5–7] Based on our current understanding, while we are able to choose the values of most device parameters, we are not able to predict the optimal amount of doping for a given design. In this letter, we present a systematic study of the effect of doping on the performance of THz QCLs.

The active region of the QCL wafer, similar to Ref. 6, is based on a four-well module design in which the THz generating transition is from a pair of anticrossed double-well states, the longitudinal-optical (LO) phonon-mediated relaxation occurs in a wide and doped subsequent well, and the injection to the following double well is from an undoped well. A schematic of the conduction-band profile is shown on the left part of Fig. 1, together with the calculated squared wave functions of the most important states. In order to isolate the effects solely due to doping, it is crucial to keep all the other parameters, including Al fraction and layer (well and barrier) thicknesses, unchanged while varying the doping concentration. This would be difficult to ensure by growing different wafers, due to the fluctuations in Ga and Al fluxes during the 20 h growth time for the present QCL design. To eliminate such uncertainty, a special molecular-beam epitaxy (MBE) growth procedure was employed. We used δ-doping with Si at the center of the 153-Å-thick "phonon" well and stopped the wafer rotation only during the doping, each time precisely aligning the wafer's $[01\bar{1}]$ crystallographic direction along the Si cell azimuthal orientation (see Fig. 1). This resulted in a nearly linear gradient of the doping concentration across the 3 in. wafer which had otherwise identical layer thicknesses and aluminum fraction. X-ray measurements indicated that the uniformity of layer thicknesses across the wafers was within ±0.5%, while the Al fraction uniformity was better than ±0.0003. The wafer was grown on a semi-insulating GaAs substrate with 176 cascaded four-well modules made of GaAs wells and $Al_{0.15}Ga_{0.85}As$ barriers. Cladding and contact layers were the same as those in Ref. 6, except that the etch-stop layer was 0.1-μm-thick AlAs and the lower contact layer was 0.1-μm-thick n^+ GaAs, doped with Si to 5.0×10^{18} cm^{-3}. Beginning with the injection barrier, the layer thicknesses of the four-well module are **54**/78/**24**/64/**38**/1<u>5</u>3/**35**/88 Å; where the barrier layers are shown in bold and the doped layer is underlined. A schematic of the wafer and the positions of the measured samples are shown on the right part of Fig. 1.

Four pieces (labeled A–D) were used for this study. By secondary ion mass spectroscopy (SIMS) measurements, their δ-doping densities were determined to be 3.2×10^{10} cm^{-2} (Sample A), 3.6×10^{10} cm^{-2} (B), 4.2×10^{10} cm^{-2} (C), and 4.8×10^{10} cm^{-2} (D), respectively. The

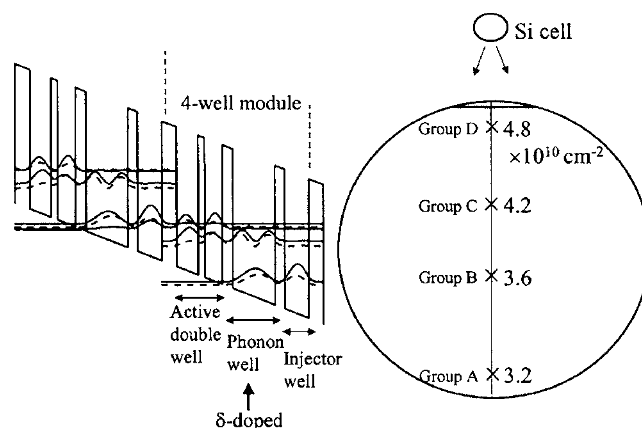

FIG. 1. Schematic conduction band profile, calculated wave functions, and schematic wafer layout.

[a)]Electronic mail: h.c.liu@nrc.ca

© 2005 American Institute of Physics
Downloaded 27 Sep 2005 to 18.62.4.5. Redistribution subject to AIP license or copyright, see http://apl.aip.org/apl/copyright.jsp

TABLE I. Doping parameters and measured results for a set of four samples. The average density is the value of the 2D δ-doping divided by the total module thickness (534 Å), representing the average carrier density. The last two rows list the measured threshold current density at 10 K and in the infinite cavity length limit, and the maximum lasing temperature.

Sample	A	B	C	D
δ-doping density (cm^{-2})	3.2×10^{10}	3.6×10^{10}	4.2×10^{10}	4.8×10^{10}
Average doping density (cm^{-3})	6.0×10^{15}	6.7×10^{15}	7.9×10^{15}	9.0×10^{15}
Threshold current density (A/cm^2)	255	408	580	800
Maximum lasing temperature (K)	90	109	88	79

nearly linear variation across the wafer is in good agreement with theoretical modeling[8] done prior to the growth. The δ-doping used here is not expected to result in any difference from the uniform doping as in Refs. 3, 4, and 6. The doping density and key measured results are listed in Table I. Although SIMS measurements give us values for the Si concentration in the material, the amphoteric nature of Si in GaAs along with possible compensation by residual acceptors may result in a net electron concentration being considerably lower than Si concentration. We have therefore carried out electrochemical capacitance-voltage (ECV) profiling on two pieces of the wafer having the highest and lowest Si concentrations. The ECV measured carrier densities are 5 and 7×10^{15} cm^{-3} for the lowest and the highest doping pieces, respectively. The ratio between the ECV inferred highest and lowest densities is 1.4. These values are compared with those for Samples A and D listed in Table I (6.0 and 9.0×10^{15} cm^{-3}). The ratio between the SIMS determined values for Samples A and D is 1.5. Considering the uncertainties involved in ECV and SIMS measurements, the agreement (1.5 for SIMS versus 1.4 for ECV) is very good, showing that with the growth conditions chosen for the present wafer Si atoms occupy mostly the donor sites and the residual doping for the material is comparatively low.

The samples (A to D) were fabricated into high-confinement metal-metal waveguides using In–Au metallic wafer bonding as described in Ref. 6. Lasers with various ridge widths (wet etched and ranged from 40 to 200 μm) and cavity lengths (1–2 mm) were tested. All lasers were biased in pulsed mode with a pulse width of 1 μs and repetition rate of 1 kHz.

Electrical and optical characteristics of the fabricated QCLs were measured at cryogenic heat-sink temperatures (10 to 120 K). Figure 2(a) shows the temperature-dependent light versus current density curves of one device cut from Sample C. The threshold current density J_{th} increases with temperature. Using the phenomenological expression $J_{th} = J_0 + J_1 \exp(T/T_0)$ to fit the data, we obtained a characteristic temperature of $T_0 = 32.5$ K. The inset to Fig. 2 shows a typical lasing spectrum measured at 10 K, which is peaked at 103.58 μm in a wavelength corresponding to 2.90 THz in frequency. Figure 2(b) shows the measured current versus voltage characteristics at various temperatures.

Figure 3 shows the threshold current density versus the heat-sink temperature for different groups of devices. Different curves within each group result from devices with different cavity lengths and ridge widths, respectively. It is clear

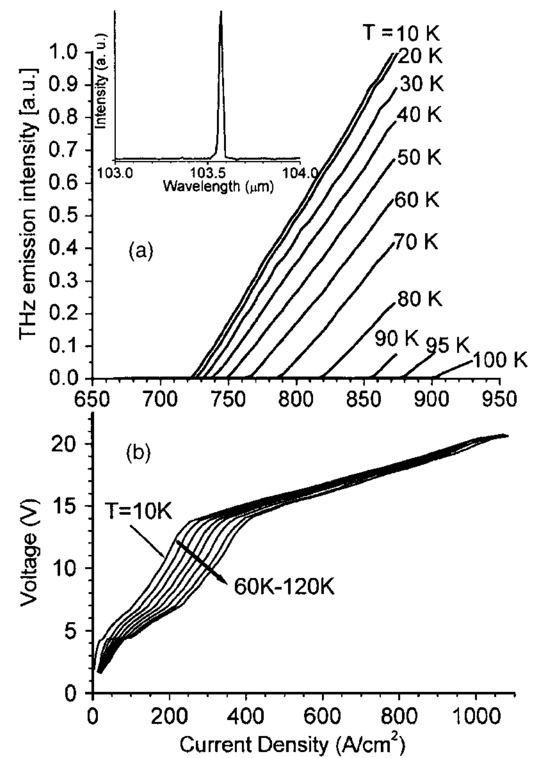

FIG. 2. Lasing light-current (a) and voltage-current (b) curves at different temperatures. The inset shows a lasing spectrum, peaked at 103.58 μm. The device was biased at 632 A/cm^2 in pulsed mode at 10 K.

that devices with the lowest δ-doping concentration (Sample A) have the lowest threshold current density, while J_{th} is the highest for those with the highest δ-doping concentration (Sample D). This stands in contrast to results in Ref. 9 for midinfrared QCLs, where the dependence of J_{th} on doping was nonmonotonic. Figure 4 plots the threshold current density at 10 K for devices with different cavity lengths as a function of the reciprocal cavity length $1/L$. The thresholds in the limit of infinite cavity length $(1/L \rightarrow 0)$ are given in Table I. The behavior in Figs. 3 and 4 is consistent with a monotonic increase of the waveguide loss as the doping is increased. Unfortunately, we cannot extract the waveguide loss reliably as it would need an accurate determination of the transparency current density and the parasitic current as well as the mirror loss. For the present metal-metal waveguide, similar to a microstrip transmission line, the mirror loss is more complicated to simulate than the usual dielectric waveguide. Recent electromagnetic simulations of Kohen

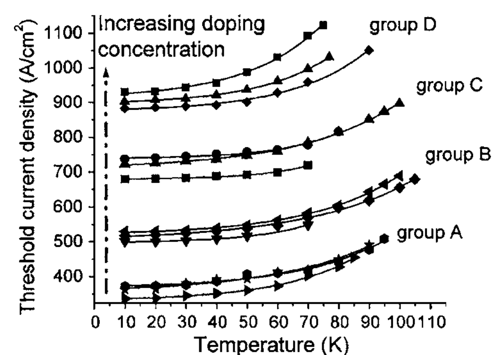

FIG. 3. Threshold current density as a function of heat-sink temperature for the four groups of devices with different geometrical configurations (cavity length and ridge width).

Downloaded 27 Sep 2005 to 18.62.4.5. Redistribution subject to AIP license or copyright, see http://apl.aip.org/apl/copyright.jsp

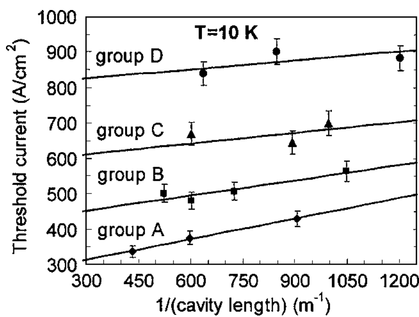

FIG. 4. Threshold current density at 10 K and in pulsed mode as a function of reciprocal cavity length. The symbols show experimental data and the solid lines are linear fits.

et al.[10] predicted a reflectivity value in the range of 0.76–0.85 very different from that of about 0.3 calculated by an effective index of about 3.5.

So far, the general trends of the results are not surprising: Increasing doping results in an increase in free-carrier absorption and waveguide loss and therefore an increase in the threshold current. Although a lower doping leads to a lower threshold, it is obvious that the limit of zero doping is a useless situation (zero gain and therefore no lasing). In the high doping limit, it is also obvious that a very high threshold would render the device inoperable. There must be therefore an optimum region of doping for certain device characteristics. One of the most important figures of merit is the maximum operating temperature $T_{\max}$, which depends not only on the characteristic temperature T_0, but the range of current densities for which lasing occurs, i.e., $J_{\max}-J_{\mathrm{th}}$, where $J_{\max}$ is the maximum current density for which lasing occurs. Beyond this $J_{\max}$, subband misalignment happens and lasing ceases. Figure 5 shows the observed maximum lasing temperature $T_{\max}$ of the four groups of QCLs as a function of δ-doping density. It clearly shows the existence of an optimum δ-doping density ($\sim 3.6\times 10^{10}$ cm^{-2}). Note that each of the experimental points in Fig. 5 is the average of results from several devices and the error bars are the results of a statistical analysis. In addition to $T_{\max}$, we also analyzed T_0 for all devices, but no trend was found.

Although the observed results are not unexpected, we do not have a quantitative explanation. We hope that advances in modeling[11–13] would, in the future, provide the interpretation and the predicting power for the design of THz QCLs. Our results are somewhat different from those measured on a set of midinfrared QCLs,[9] where a minimum in the threshold as a function of doping was observed. However, in addition to the very different wavelengths ($\sim$10 μm there versus 103 μm here) the device design and parameters of that experiment were quite different (e.g., more than ten times higher doping concentration). We note at least one key difference in the physical process: For midinfrared QCLs, the radiative energy level separation is greater than the LO-phonon energy and the upper-state lifetime is dominated by LO-phonon scattering, which is relatively independent of the electron distribution and injection level. As a result, a larger doping should increase both J_{th} and $J_{\max}$ linearly. However, for THz QCLs, the radiative energy level separation is less than the LO-phonon energy, and fast LO-phonon scattering is only available to carriers that have sufficient kinetic energy.[11,12] Hence, the upper-state lifetime sensitively depends on the injection level which changes the electron temperature and population on the upper level. Thus, even though the threshold population inversion may be simply linear with the doping level (which is proportional to the cavity loss), the threshold current density likely increases faster. Hence, the issue of optimum doping. This interdependence of relaxation rate on injection level is the main reason why the linear rate-equation approach, which has worked well for midinfrared QCLs, is not applicable for THz QCLs. Clearly more investigations are called for.

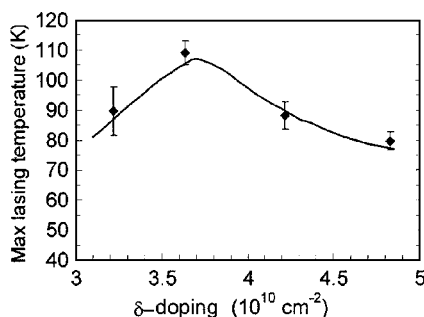

FIG. 5. Measured maximum lasing temperature as a function of δ-doping concentration. The maximum temperature was measured in pulsed mode (pulse width 1 μs and repetition rate 1 kHz) by increasing heat-sink temperature until the lasing operation could not be observed. The symbols are measured results and the curve is a guide for the eyes.

The authors thank B. Aslan, E. Dupont, P. D. Grant, H. Luo, and C. Y. Song for helpful discussions, P. Barrios, A. Bezinger, R. Dudek, J. Froemel, M. Malloy, P. Marshall, and R. Wang for technical assistance, G. I. Sproule for SIMS measurements, and E. Fortin of University of Ottawa for indium deposition. J. Boudet (Ecole Polytechnique-France) contributed in the beginning phase of this project. For the NRC part, this work was supported in part by the NRC GHI program, for the Shanghai part by the National Fund for Distinguished Young Scholars (60425415) and the major project of the National Science Foundation of China (10390162), and for the MIT part by AFOSR, NASA, and NSF.

[1] R. Köhler, A. Treicucci, F. Beltram, H. E. Beere, E. H. Lienfield, A. G. Davis, D. A. Ritchie, R. C. Iotti, and F. Rossi, Nature (London) **417**, 156 (2002).
[2] M. Rochat, L. Ajili, H. Willenberg, J. Faist, H. Beere, G. Davies, E. Linfield, and D. Ritchie, Appl. Phys. Lett. **81**, 1381 (2002).
[3] B. S. Williams, H. Callebaut, S. Kumar, Q. Hu, and J. L. Reno, Appl. Phys. Lett. **83**, 2124 (2003).
[4] B. S. Williams, S. Kumar, Q. Hu, and J. L. Reno, Opt. Express **13**, 3331 (2005).
[5] R. Köhler, A. Tredicucci, F. Beltram, H. E. Beere, E. H. Linfield, A. G. Davies, D. A. Ritchie, S. S. Dhillon, and C. Sirtori, Appl. Phys. Lett. **82**, 1518 (2003).
[6] S. Kumar, B. S. Williams, S. Kohen, Q. Hu, and J. L. Reno, Appl. Phys. Lett. **84**, 2494 (2004).
[7] S. Barbieri, J. Alton, H. E. Beere, J. Fowler, E. H. Linfield, and D. A. Ritchie, Appl. Phys. Lett. **85**, 1674 (2004).
[8] Z. R. Wasilewski, G. C. Aers, A. J. SpringThorpe, and C. J. Miner, J. Vac. Sci. Technol. B **9**, 120 (1991).
[9] M. Giehler, R. Hey, H. Kostial, S. Cronenberg, T. Ohtsuka, L. Schrottke, and H. T. Grahn, Appl. Phys. Lett. **82**, 671 (2003).
[10] S. Kohen, B. S. Williams, and Q. Hu, J. Appl. Phys. **97**, 053106 (2005).
[11] H. Callebaut, S. Kumar, B. S. Williams, Q. Hu, and J. L. Reno, Appl. Phys. Lett. **84**, 645 (2004).
[12] D. Indjin, P. Harrison, R. W. Kelsall, and Z. Ikonić, IEEE Photonics Technol. Lett. **15**, 15 (2003).
[13] R. C. Iotti and F. Rossi, Phys. Rev. Lett. **87**, 146603 (2001).

Downloaded 27 Sep 2005 to 18.62.4.5. Redistribution subject to AIP license or copyright, see http://apl.aip.org/apl/copyright.jsp